Influence of deposition time variation and mass concentration of MgO on the corrosion response and microstructure of Zn-MgO-Al_2O_3 electroplated mild steel

O. O. Ajide[1], P. Amunachugo[1], O. A. Aogo[2] and I. G. Akande[3*]

[1] Department of Mechanical Engineering, University of Ibadan, Ibadan, Nigeria

[2] Department of Research and Development, Standard Connections Limited, Nigeria

[3] Department of Automotive Engineering, University of Ibadan, Ibadan, Nigeria

[*]Corresponding Author's emails: ig.akande@ui.edu.ng, aigodwin2015@gmail.com

Lead Author's emails: ooe.ajide@ui.edu.ng, ooe.ajide@gmail.com

Abstract

Zinc electroplated mild steels have been used extensively in automotive, marine and petrochemical industries. However, their vulnerability to corrosion and structural failure over time has required the inclusion of metallic oxide to enhance the coating properties. This work examined the influence of time variation on the corrosion response and microstructure of Zn-MgO-Al_2O_3 electroplated mild steel. The corrosion properties of the coating were examined using the potentiodynamic polarization experiment in a three-electrode system, employing a 3.5% wt. NaCl solution. The microstructure of the coated samples was examined using the Scanning Electron Microscope (SEM). The control (uncoated sample) exhibited the least corrosion resistance, with the corrosion rate (Cr) and corrosion current density (j_{ocorr}) of 20.707 mm/year and 1782 μA/cm^2, respectively. The steel coated with Zn-MgO30-Al_2O_3 (20 mins) exhibited the optimum corrosion resistance, with the Cr and j_{corr} of 1.0521 mm/year and 90.51 μA/cm^2, respectively. The foregoing indicated that the coating minimized the attack on the steel surface by the corrosive medium. The SEM images indicated that the coatings were well dispersed on the steel surface, exhibiting minimal cracks and pores, revealing that the coating constituents are compatible. The variation in the deposition time and mass concentration of MgO had a significant effect on corrosion resistance and the microstructure of the coatings. Hence, the coating could be employed for advanced applications such as automotive, marine, petrochemical and chemical storage.

Keywords: Electroplating; Corrosion-resistant; corrosion current density; Zn-MgO-Al_2O_3; Coating

1. Introduction

Steel is one of the most mass-produced metals in existence [1-3]. Steels come in different grades [4, 5]. Mild steel is a grade of steel with low hardness properties and low ultimate tensile strength [6-8]. However, it is one of the world's least expensive and readily available metals [9, 10]. The carbon content in a sample of mild steel determines its properties. The maximum carbon content of 0.25% and in most cases, varying percentages of sulphur, silicon, manganese and phosphorus e.t.c in trace amounts and iron in a large quantity are contained in mild steel [11, 12]. Mild steel is also quite malleable even when cold, unlike other types of steel [13, 14], and its low carbon content gives it some level of resistance to breakage [15, 16]. Iron, which is the major constituent of steel, is in its pure form soft and generally not useful as an engineering material. The principal method of strengthening and converting it into steel is by adding small amounts of carbon to enhance physicochemical properties [17, 18]. Steel is the most commonly employed metallic material in open-air structures and is used to make a wide range of equipment and metallic structures due to its low cost and ready availability [19-21]. The most important properties of steel are its great formability, durability, good yield strength and good thermal conductivity.

However, for steel components exposed to the atmosphere and other harsh environments, it is critical to coat the steel for corrosion protection [22, 23]. It is estimated that annual loss and damage due to corrosion in the United Kingdom costs about £5000 million, and approximately one ton of steel is lost through corrosion every 90 seconds [24]. Ferrous-based alloys like steel are generally susceptible to corrosion and wear. Thus, limiting their use in marine, automotive and petrol chemical environments [25, 26]. To enhance the corrosion resistance of steel alloys, the use of zinc as sacrificial coatings in the electroplating of ferrous substrates has been well reported [27-29]. However, one of its major limitations is that it degrades with time as it exposes to the atmosphere due to corrosion [30-32]. Corrosion of steel is an electrochemical process, in which iron (Fe) is taken from steel, dissolved in the surrounding fluid, and deposited as a red-brown hydrated metal oxide in any environment [33, 34]. Hence, there is a need to further enhance the corrosion resistance of the alloys by the inclusion of alloying elements. Recent advances show that the electroplating characteristics of zinc can be modified by the addition of some alloying elements, utilizing surface engineering techniques [35-37].

Surface engineering has been classified as both a science and the art of improvement for surfaces of various materials [38-39]. The application of the surface coatings may be by electrochemical or electrolytic means usually for protective purposes and also for improving the appearance of the metal and also to improve mechanical characteristics and other required properties [40, 41]. The surface coatings can either be non-metallic or metallic coatings. In recent years, technological improvements have made protective metallic or non-metallic coatings one of the most commonly used systems of corrosion control [42, 43]. The intrinsic properties of these coatings make mild steel relevant for structural applications, automobile bodies and cans, especially after being subjected to treatment and protection by surface engineers. As is often the case, the coating materials are selected based on the desired properties. For instance, in this work, zinc is used because it has better corrosion resistance than steel. It has been employed for the galvanizing of steel [44, 45]. Galvanizing, a surface coating process uses zinc (Zn) as its major coating element to protect metals from corrosion. On the electrochemical series, zinc has a lower reduction potential (E^o = -0.76V) than Iron (E^o = -0.44V), making zinc more easily oxidized than iron and thus more reactive [46-48]. Because zinc is more reactive, when exposed to the atmosphere, Zn reacts with oxygen to form ZnO [49, 50]. Aluminium oxide (Al_2O_3) also known as alumina is chemically inert and insoluble in water. It has a very high melting of 2072 °C [51, 52], indicating that it can aid the enhancement of corrosion and mechanical properties. Magnesium oxide (MgO) powder has also been reportedly employed by several authors to enhance the corrosion of metals due to its ability to form a passivation layer, which prevents the ingression of corrosive ions into the active sites of the metal [53, 54]. Therefore, this research investigated the effect of time variation and concentration of MgO on the corrosion response and microstructure of Zn-MgO-Al_2O_3 coated mild steel.

2. Experimental Procedures

2.1 Materials

The substrates used in this work were sectioned rectangular mild steel plates with a dimension of 40 mm × 40 mm × 2 mm, procured in Ogun state, Nigeria. Zinc anode of dimension 80 mm × 60 mm × 20 mm, also procured in Ogun state, Nigeria, was also used in this study. The weight percentage of elements in the mild steel used is indicated in Table 1. The other co-deposited materials such as MgO and Al_2O_3 were equally purchased in Ogun state in powdery form.

Table 1: Percentage composition of mild steel

Element	Mn	C	S	Si	P	Ni	Al	Fe
Composition	0.43	0.16	0.033	0.16	0.02	0.008	0.007	Bal.

2.2 Bath Formulation

The deposition bath was prepared using reagents indicated in Table 2. The proportion of the reagents inclusion in the bath is equally indicated. The process parameters such as temperature, pH, voltage, stirring rate and deposition time are also indicated. The KCl, NaCl and $ZnCl_2$ form the basic component of the bath, which aids the flow of current. Thus, the bath could be referred to as a chloride bath.

Table 2: Bath formulation

Composition & process perimeters	Mass concentration & magnitude of process perimeters
KCl	30 g/L
Boric Acid	10 g/L
Thiourea	10 g/L
NaCl	40 g/L
MgO	10, 20 & 30 g/L
$ZnCl_2$	30 g/L
Al_2O_3	10 g/L
pH	5.63
Voltage	0.5 V
Time	10, 15 & 20 mins
Temperature	45 ^oC
Stirring rate	250 rpm

2.3 Pre-coating Process

The pre-coating procedure involves polishing the mild steel samples surface with grades of emery paper whose grit range from 120 to 180. To get rid of organic oxides and contaminants, pickling of the steel surface was done in a 10 percent HCl solution. Ultimately, the steel samples were washed in distilled water before the initiation of coating. The cross-sections of the polished samples are indicated in Figure 1.

Figure 1: Polished mild steel samples

2.4 The Coating Process

During the coating process, two zinc metals were used as anodes, while mild steel was the cathode. The cathode was positioned 3 cm between the anodes in the deposition bath. The content of the bath was heated to a constant temperature of 45 ^{o}C and stirred at a stirring rate of 250 rpm to allow for mass flow of particles or electrophoresis. The constant agitation of the bath was also to ensure the homogeneous dispersion of particles on the surface of the steel substrates. The coating was achieved at the varying temperature of 10, 15 and 20 minutes and varying mass concentrations of MgO (10, 20 and 30 g/L). The deposition voltage was held constant at 0.5 V and pH of 5.63. After each coating, the coated samples' surfaces were slightly rinsed in distilled water to remove the salty solution from the coating and then allowed to dry in natural air. The cross sections of the coated mild steel samples are indicated in Figure 2.

Figure 2: cross sections of coated mild steel samples

2.4 Characterization of the Uncoated and Coated samples

2.4.1 Electrochemical experiment

Before the characterization of the samples, the uncoated and coated samples were sectioned to the dimension of 10 mm × 10 mm × 2 mm. For the electrochemical test (potentiodynamic polarization experiment), the 10 mm × 10 mm × 2 mm specimen (working electrode) was connected to a copper wire and embedded in an epoxy resin, leaving an exposed area of 10 × 10 mm^2. This was linked to the reference electrode (Ag/AgCl electrode) and a counter electrode (graphite electrode), which were in turn connected to a computer-controlled metrohm-Autolab PGSTAT 101. The analysis was performed using Nova 2.1 software. The electrodes were immersed in 3.5% NaCl solution, and the potentiodynamic polarization experiment was run at the start and end potentials of -1.5 and 1.5 V, respectively, at a scan rate of 5 mV/s. The open circuit potentials of the samples were also evaluated. Using Equations 1 and 2, the corrosion rate and polarization resistance were estimated, respectively, following the ASTM G102 standard. The coating efficiency (C.E) was also estimated using Equation 3.

$$\mathrm{Cr} = (0.00327 \times j_{corr} \times \mathrm{eq.w}) / \ell \quad (1)$$

$$\mathrm{Pr} = 2.303 b_a b_c / j_{corr} (b_a + b_c) \quad (2)$$

$$\mathrm{C.E} = (1 - j_{corr} / j_{ocorr}) \times 100 \quad (3)$$

Where 0.00327 is the constant, ℓ is the density of samples in g/cm^3, j_{ocorr} and j_{corr} in A/cm^2 are the corrosion current density of the uncoated and coated steel, respectively, eq.w is the equivalent weight of samples in grams, while bc and ba are the cathodic and anodic slopes, respectively.

2.4.2 Microstructural examination of samples

The microstructural examination of the samples was carried out using a Scanning Electron Microscope (SEM). The SEM images were captured at the magnification of 200 times the original samples. The detector of the SEM used was HD backscattered detector (HDBSD). The samples were subjected to an extra high tension (EHT) of 20.00 kV and high vacuum mode.

3. Results and Discussion

3.1 Analysis Electrochemical (Corrosion) Performance of the Samples

3.1.1 Potentiodynamic polarization data of samples

The corrosion rate (Cr), corrosion current density (j_{corr} and j_{ocorr}) and polarization resistance (Pr) of the uncoated and coated samples are shown in Table 3. The Zn-MgO30-Al_2O_3 (20 mins) sample exhibited the best corrosion resistance, relative to the other test samples. The Zn-MgO30-Al_2O_3 (20 mins) coating is adjudged the best corrosion-resisting coating in the test medium due to the least Cr of 1.0521 mm/year, lowest j_{corr} of 90.51 $\mu A/cm^2$ and highest Pr of 292.15 Ω. These parameters showed that the Zn-MgO30-Al_2O_3 (20 mins) coating offered the best resistance to the entrance of the corrosive ions from the 3.5% NaCl solution into the surface and the active sites of the base metal (mild steel) [55, 56]. It is also worthy of note that the control sample (uncoated mild steel sample) possessed the highest Cr of 20.707 mm/year, the utmost j_{ocorr} of 1782 $\mu A/cm^2$ and the least Pr of 34.47 Ω. These values indicated that the control sample offered the least resistance effect to the deterioration of the corrosive ions [57]. It was further observed that the mass concentration of MgO and the coating time played vital roles in the corrosion-resisting performance of the coatings. For instance, Zn-MgO10-Al_2O_3 (20 mins) coating achieved in 20 minutes exhibited the Cr of 6.4252 mm/year, while Zn-MgO10-Al_2O_3 (15 mins) and Zn-MgO10-Al_2O_3 (10 mins) coating exhibited higher Cr of 6.5122 and 7.7608 mm/year, respectively. In the same vein, Zn-MgO20-Al_2O_3 (20 mins) coating possessed superior corrosion resistance or lower corrosion rate compared to Zn-MgO20-Al_2O_3 (15 mins) and Zn-MgO20-Al_2O_3 (10 mins) coatings. Similarly, Zn-MgO30-Al_2O_3 (20 mins) coating possessed superior corrosion performance, relative Zn-MgO30-Al_2O_3 (15 mins) and Zn-MgO30-Al_2O_3 (10 mins) coatings. It was therefore observed that in each of the three coating phases (Zn-MgO10-Al_2O_3, Zn-MgO20-Al_2O_3 and Zn-MgO30-Al_2O_3), the corrosion performance increases with the increase in the deposition time, as also reported by Li et al., Dai et al. [58, 59]. A similar trend was also obviously observed with an increase in mass concentration, where the Zn-MgO30-Al_2O_3 (15 mins) coating exhibited superior corrosion properties than the Zn-MgO20-Al_2O_3 (15 mins) coating, Zn-MgO20-Al_2O_3 (10 mins) coating than Zn-MgO10-Al_2O_3 (10 mins) coating e.t.c. despite being subjected to the same deposition time. This type of occurrence was also reported by Zhou and Kong, Fayomi et al. [60, 61].

Table 3: Potentiodynamic polarization data of samples

Sample	**E_{corr} (V)**	**j_{ocorr} & j_{corr} (μA/cm²)**	**Cr (mm/year)**	**Pr (Ω)**
Control	-1.2994	1782	20.707	34.47
Zn-MgO10-Al_2O_3 (10 mins)	-1.0830	667.98	7.7608	88.47
Zn-MgO10-Al_2O_3 (15 mins)	-1.0283	560.43	6.5122	98.05
Zn-MgO10-Al_2O_3 (20 mins)	-1.2149	552.95	6.4252	111.09
Zn-MgO20-Al_2O_3 (10 mins)	-0.9988	474.42	5.5127	156.12
Zn-MgO20-Al_2O_3 (15 mins)	-1.1044	420.33	4.8842	167.48
Zn-MgO20-Al_2O_3 (20 mins)	-1.1055	219.43	2.5498	281.63
Zn-MgO30-Al_2O_3 (10 mins)	-1.2102	249.30	3.3215	256.35
Zn-MgO30-Al_2O_3 (15 mins)	-1.0160	178.85	2.0782	286.75
Zn-MgO30-Al_2O_3 (20 mins)	-1.2068	90.51	1.0521	292.15

3.1.2 Coating efficiency (C.E) of the deposited films

Figure 3 indicated the coating efficiency (C.E) or surface protection efficiency of the coatings. It was observed that the efficiency of the Zn-MgO-Al_2O_3 coatings increased with the deposition time. Similarly, the mass concentration of the MgO particles also enhanced the coating efficiency of the Zn-MgO-Al_2O_3 coatings. Among the Zn-MgO10-Al_2O_3 coatings, Zn-MgO10-Al_2O_3 (20 mins) coating exhibited the highest coating efficiency of 68.97%. Relative to the other Zn-MgO20-Al_2O_3 coatings, Zn-MgO20-Al_2O_3 (20 mins) possessed a superior coating efficiency of 87.69%, while the Zn-MgO30-Al_2O_3 (20 mins) coating exhibited the uppermost coating efficiency (C.E) of 94.92% compared to the other Zn-MgO30-Al_2O_3 coatings. These efficiencies indicated that the adhesiveness and protective ability of the coatings in the saline medium could be a function of the deposition time and mass concentration of particles [62].

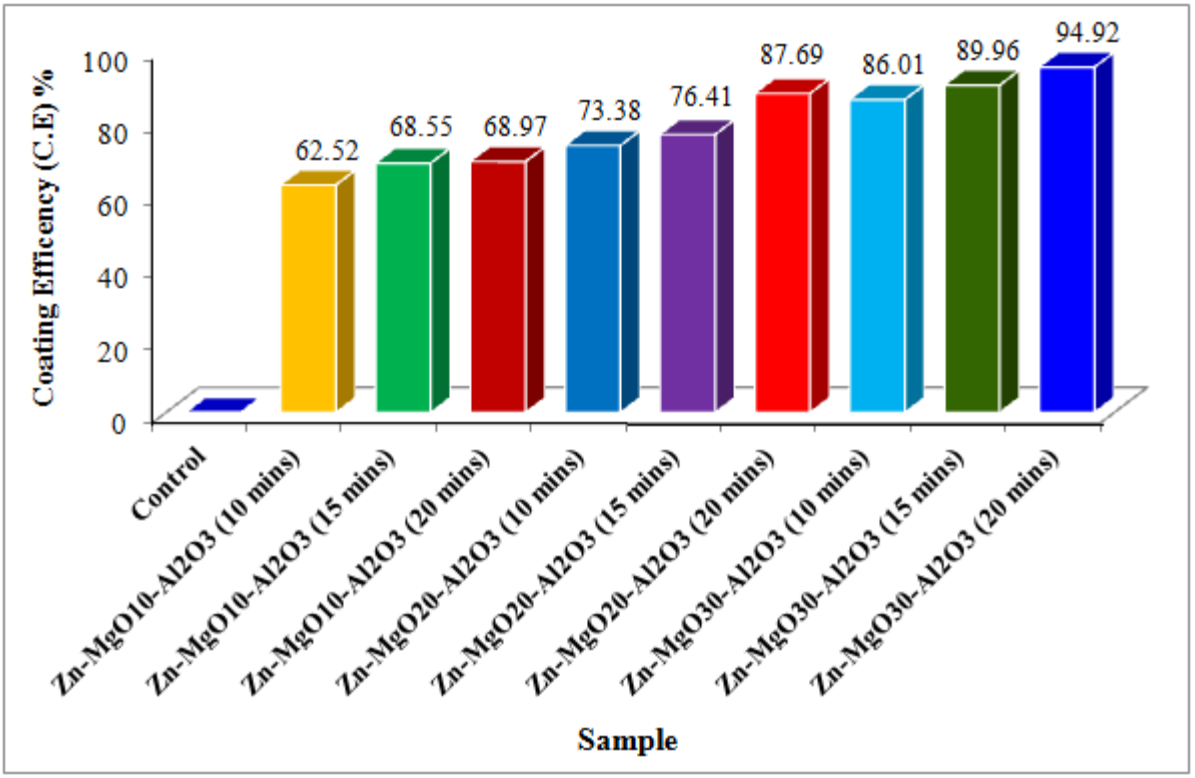

Figure 3: Coating efficiency (C.E) of the deposited films

3.1.3 Tafel plots of samples

The Tafel plots for the Zn-MgO-Al_2O_3 coated samples are shown in Figures 4-6. The Tafel plots further indicated that, for the Zn-MgO10-Al_2O_3, Zn-MgO20-Al_2O_3 and Zn-MgO30-Al_2O_3 coatings, the deposition at 20 minutes exhibited the lowest corrosion current densities. This implied that the Zn-MgO10-Al_2O_3 (20 mins), Zn-MgO20-Al_2O_3 (20 mins) and Zn-MgO30-Al_2O_3 (20 mins) coatings offer more passivation in the 3.5% NaCl solution, compared to their counterpart coatings with the same mass concentration [63, 64]. Comparing the entire coatings, the Zn-MgO30-Al_2O_3 (20 mins) coating possessed the most superior passivation The Tafel plots also indicated through the E_{corr} values that the Zn-MgO-Al_2O_3 coatings also exhibited mixed-type inhibition or protective effect on the surface of the mild steel i.e. protecting the anodic and cathodic region of the steel [65, 66].

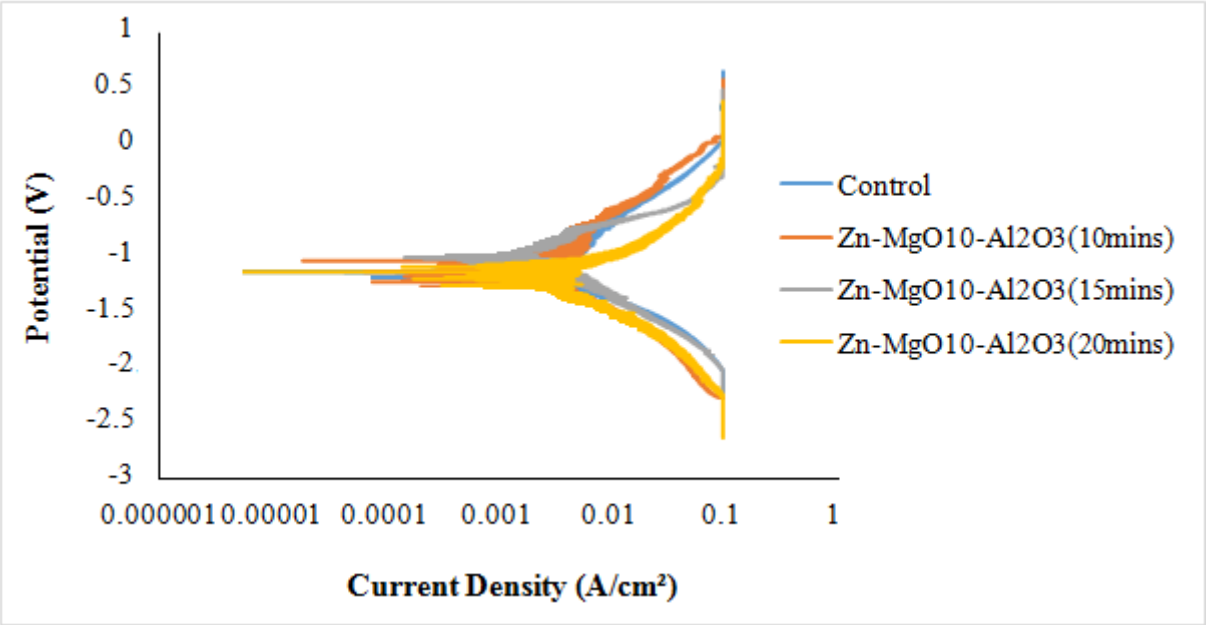

Figure 4: Tafel plots for Zn-MgO10-Al_2O_3 coated samples

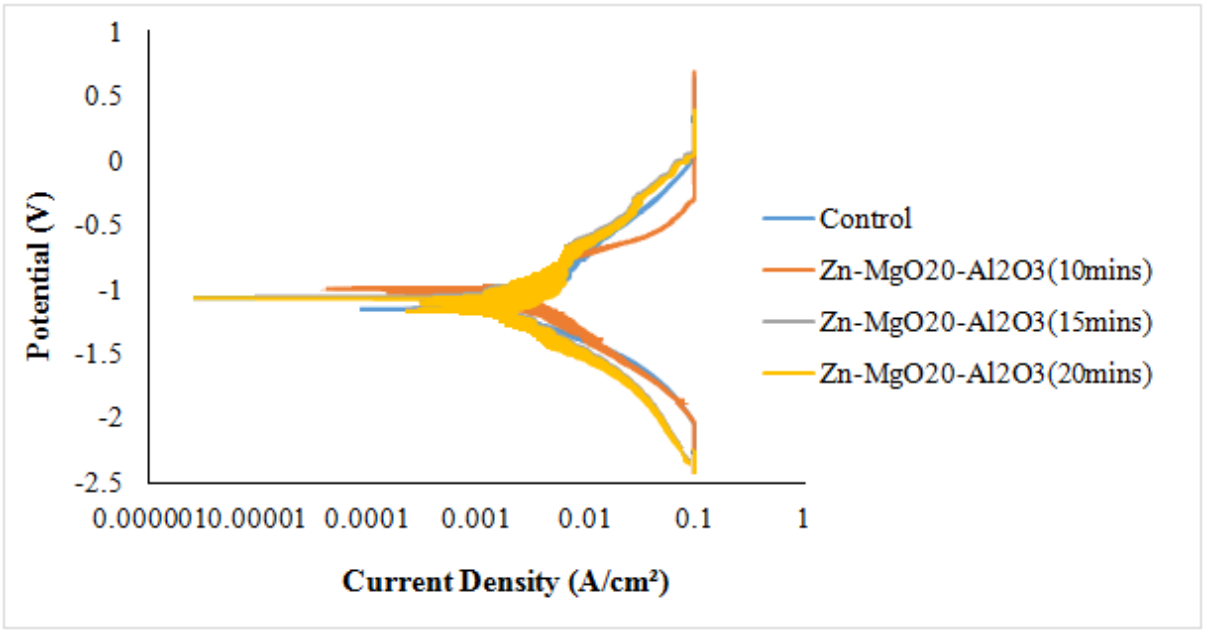

Figure 5: Tafel plots for Zn-MgO20-Al_2O_3 coated samples

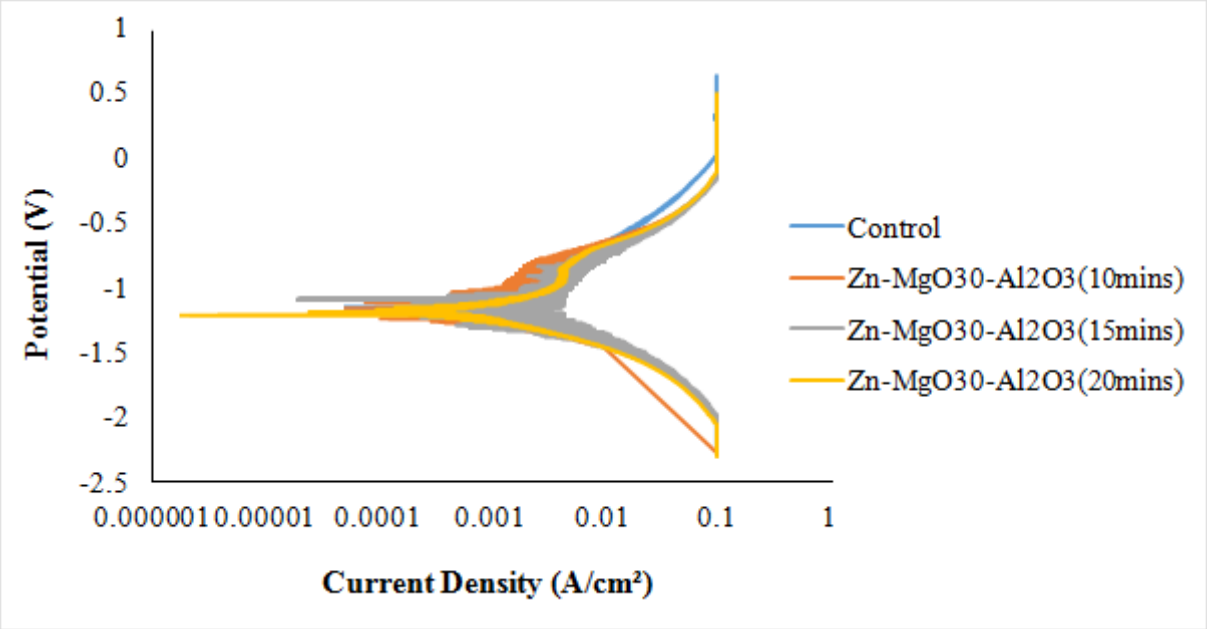

Figure 6: Tafel plots for Zn-MgO30-Al_2O_3 coated samples

3.1.4 Open-circuit potential (OCP) of samples

Figures 7-9 indicated the OCP of the Zn-MgO-Al_2O_3 coated samples. The coatings were observed to have shifted the OCP of the mild steel (control) to more negative potentials. The potential of the control was -0.69 V. This was constant for 120 seconds. This constancy in the value of the potential indicated that a steady state was reached [67]. This potential can in order words be referred to as a steady state potential. At different times, the steady state potentials of Zn-MgO10-Al_2O_3 (10 mins), Zn-MgO10-Al_2O_3 (20 mins) and Zn-MgO10-Al_2O_3 (30 mins) coatings were -0.75, -0.8 and -1.1 V, respectively. For the Zn-MgO20-Al_2O_3 coatings, the steady-state potentials of Zn-MgO20-Al_2O_3 (10 mins), Zn-MgO20-Al_2O_3 (20 mins) and Zn-MgO20-Al_2O_3 (30 mins) coatings were -0.76, -0.75 and -0.725 V, respectively. Similarly, the steady state potentials of Zn-MgO30-Al_2O_3 (10 mins), Zn-MgO30-Al_2O_3 (20 mins) and Zn-MgO30-Al_2O_3 (30 mins) coatings were -0.785, -0.745 and -0.76 V, respectively.

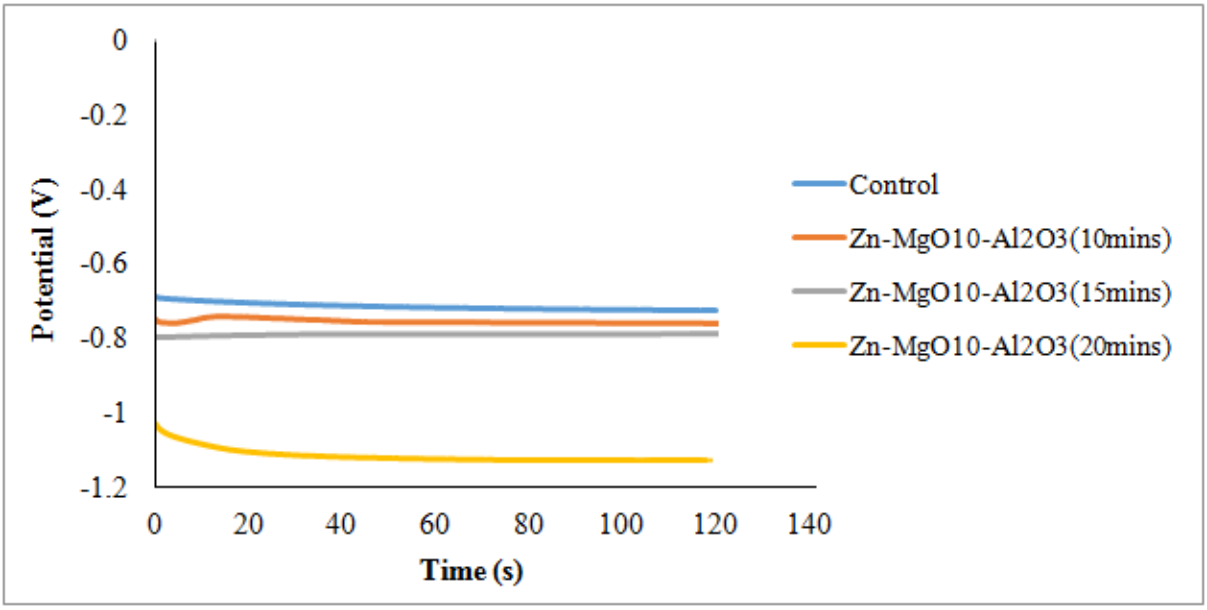

Figure 7: Open-circuit potential of Zn-MgO10-Al_2O_3 coated samples

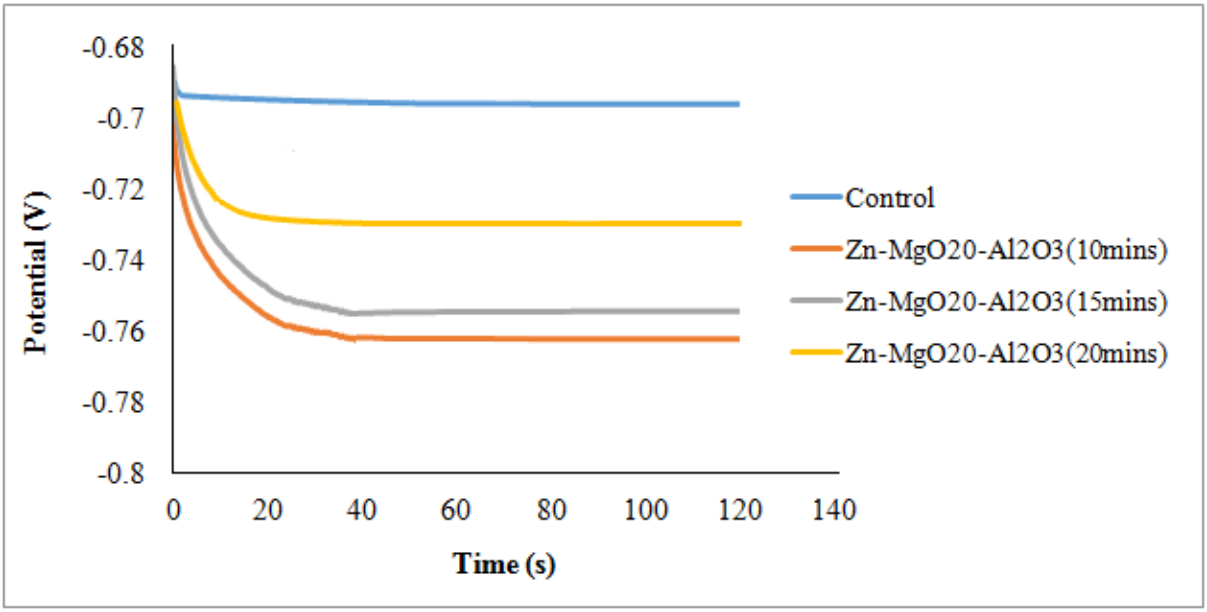

Figure 8: Open-circuit potential of Zn-MgO20-Al_2O_3 coated samples

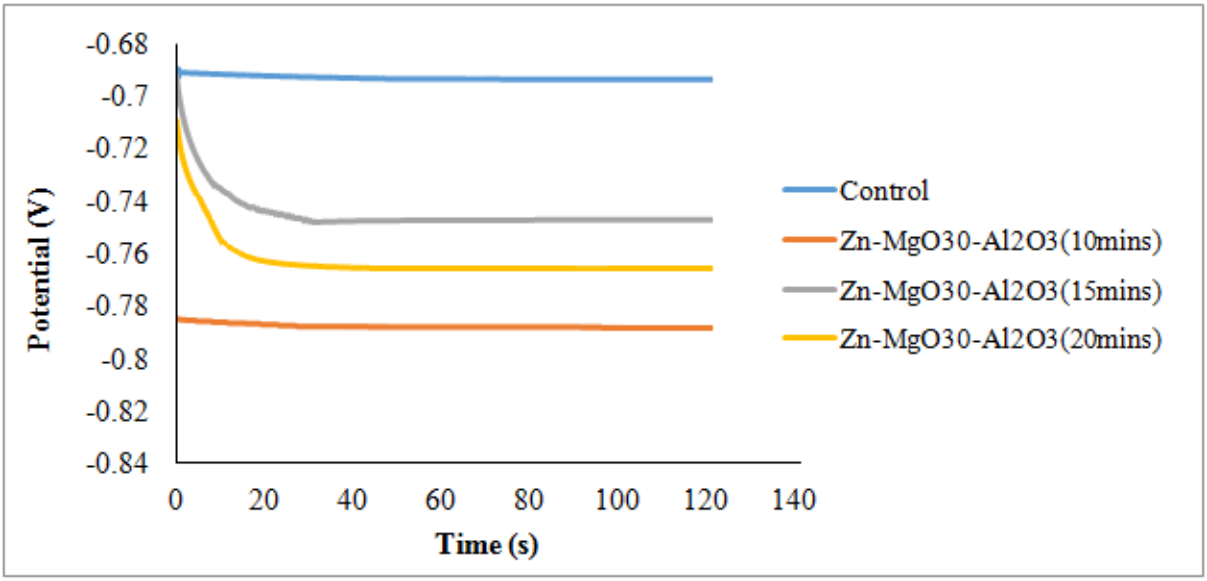

Figure 9: Open-circuit potential of Zn-MgO30-Al_2O_3 coated samples

3.2 Microstructures

The SEM images of the uncoated and coated samples are indicated in Figures 10-15. On the SEM image of the uncoated mild steel in Figure 10 was observed few puffed-up scales, indicating the initiation and propagation of corrosion products, possibly from the slight exposure to the environmental contaminants. In Figure 11, the SEM image of the Zn-MgO10-Al_2O_3 (10 mins) coated sample was observed to exhibit a granulated structure, with few clefts which could act as sites for the penetration of degrading contaminants [68, 69]. Uniform-sized grains were also observed on most sections of the sample. It is also worthy of note that the coating exhibited seemingly regular colouration, indicating the homogeneous mixture of the particles in the coating [70, 71]. As indicated in Figure 12, the SEM image of the Zn-MgO10-Al_2O_3 (15 mins) coated sample showed that the samples possessed a redefined microstructure with the predominance of flower-flake-like morphology and a portion of a dark granulated structure. Furthermore, the SEM image of Zn-MgO20-Al_2O_3 (15 mins) coated samples (see Figure 13) indicated the dispersion of larger and compact deposits of particles on the surface of the steel. The compact nature of the coating indicated the possibility of providing high corrosion resistance in a corrosive medium [72, 73]. The SEM image of the Zn-MgO20-Al_2O_3 (20 mins) coated sample shown in Figure 14 indicated that it exhibited a similar structure as the Zn-MgO20-Al_2O_3 (15 mins) coated samples. However, more particle deposition could be observed with the Zn-MgO20-Al_2O_3 (20 mins) coating. This could be attributed to the extension in the coating time. Relative to the entire samples, the Zn-MgO30-Al_2O_3 (15 mins) and Zn-MgO30-Al_2O_3 (20 mins) coatings exhibited the most refined microstructure with

unique morphologies as shown in Figures 15 and 16. However, while the Zn-MgO30-Al_2O_3 (15 mins) coated sample possessed more of a granulated structure, the Zn-MgO30-Al_2O_3 (20 mins) coated sample exhibited more of a flower-nodular-like structure. More particle dispersion and compact grain boundaries were also observed with the Zn-MgO30-Al_2O_3 (20 mins) coating, which could be the reason for the superior corrosion resistance it exhibited, compared to the other samples.

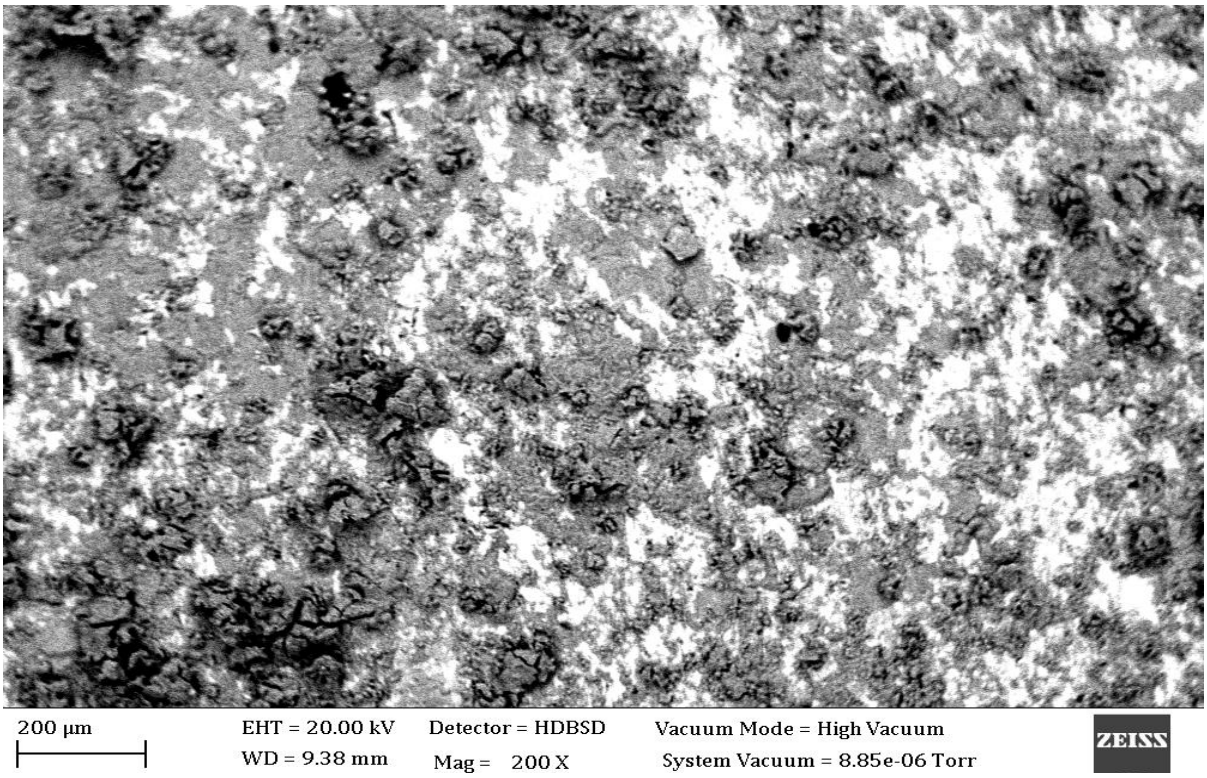

Figure 10: SEM image of the uncoated (control) sample

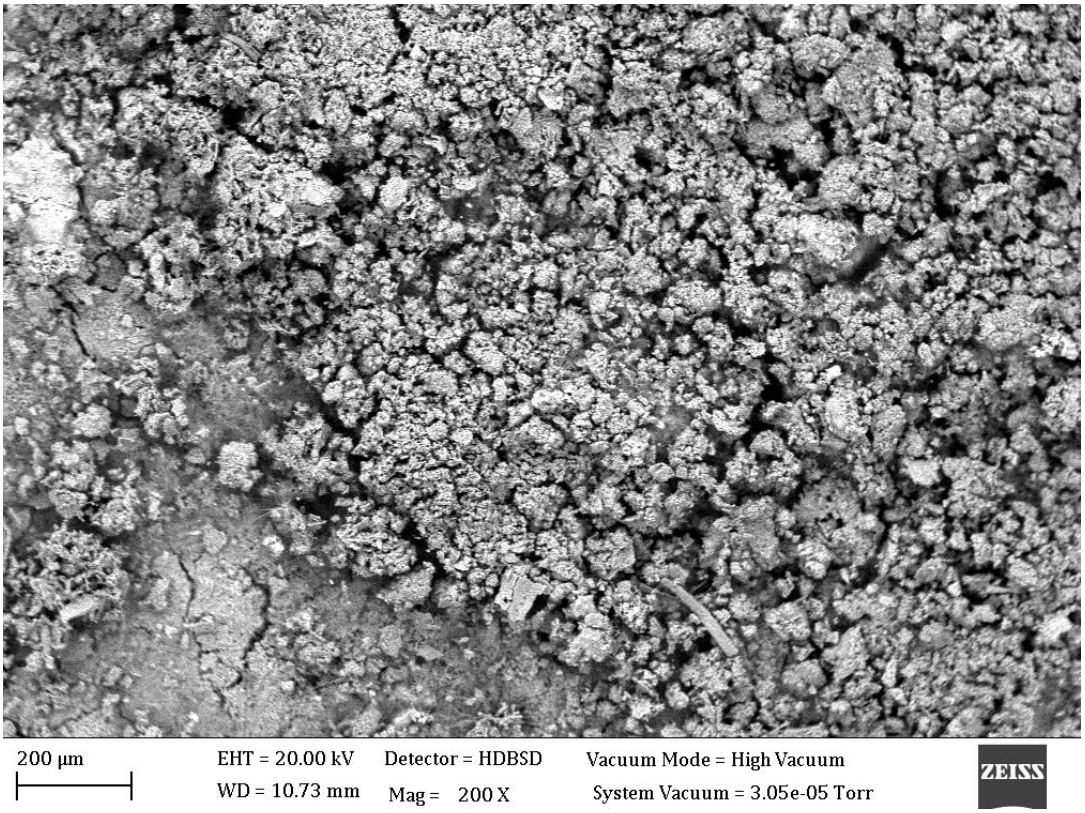

Figure 11: SEM image of Zn-MgO10-Al_2O_3 (10 mins)

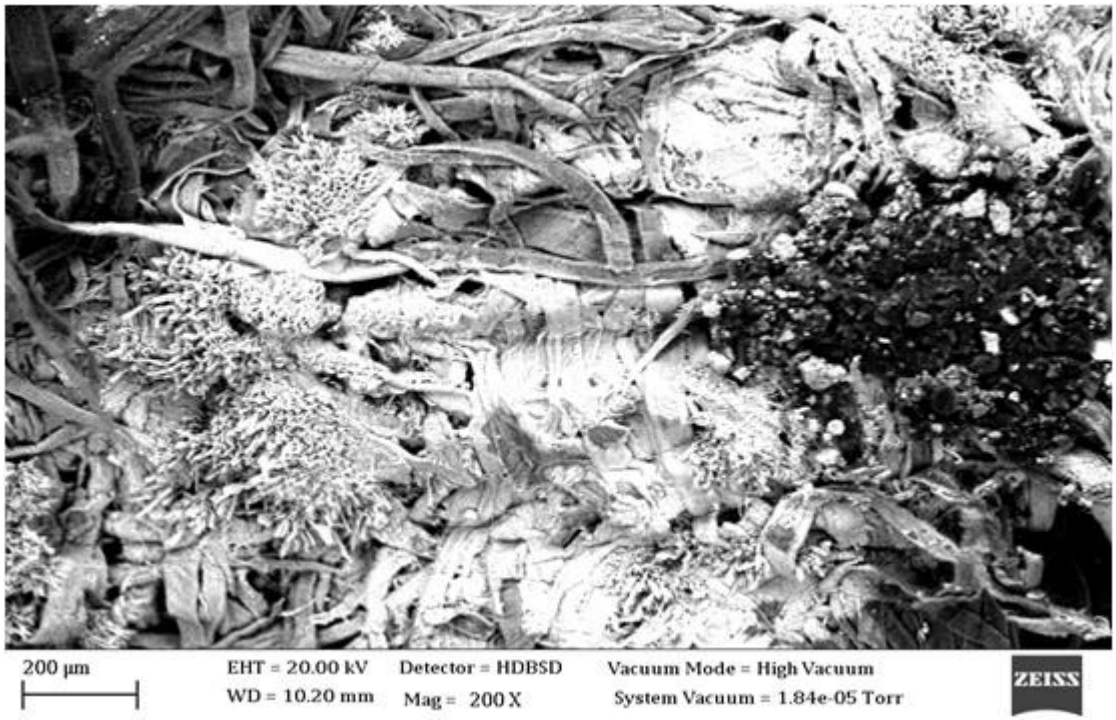

Figure 12: SEM image of Zn-MgO10-Al_2O_3 (15 mins)

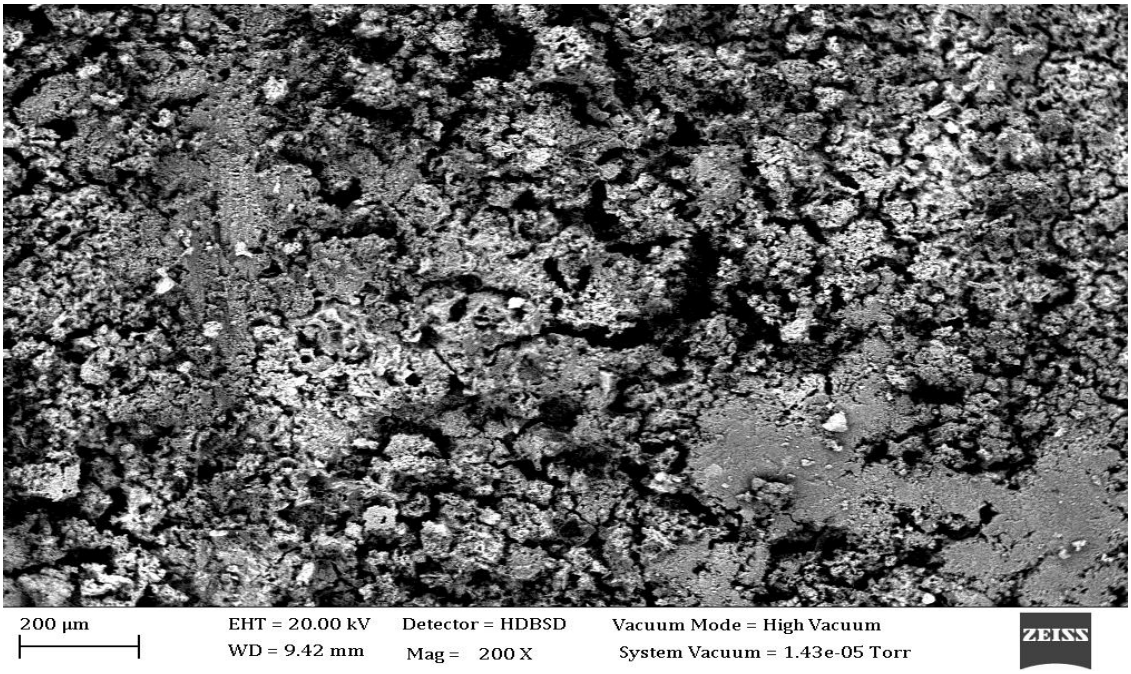

Figure 13: SEM image of Zn-MgO20-Al_2O_3 (15 mins)

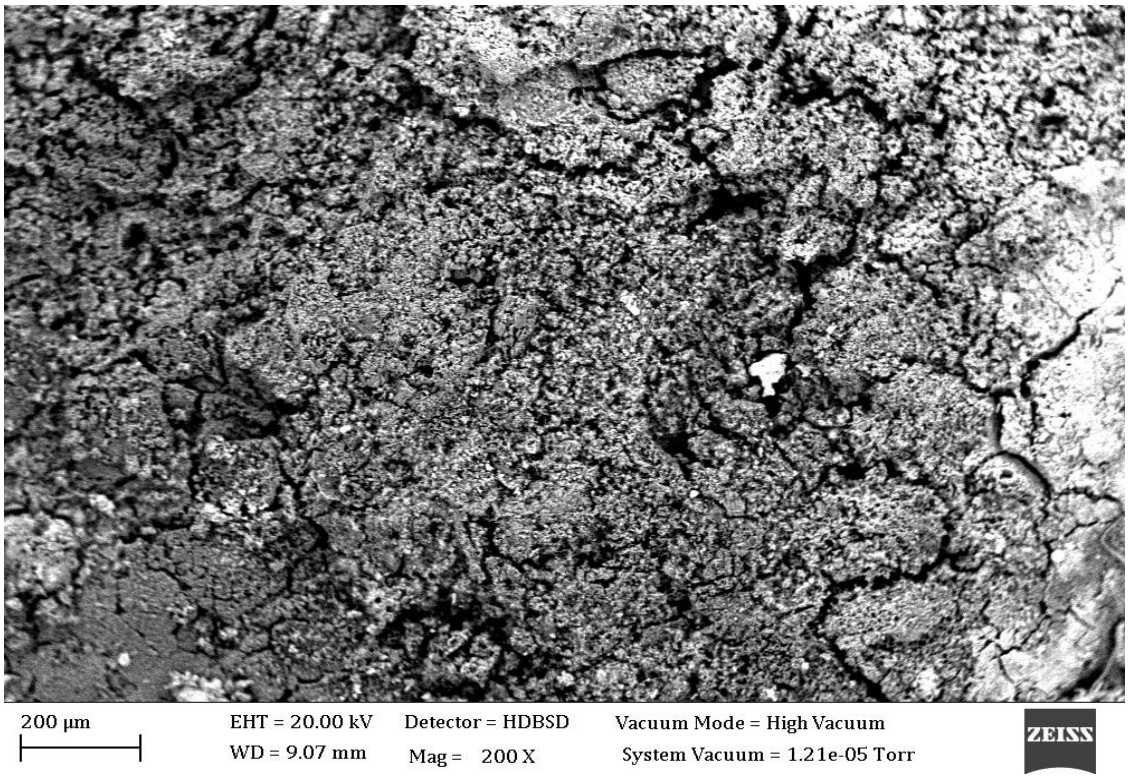

Figure 14: SEM image of Zn-MgO20-Al_2O_3 (20 mins)

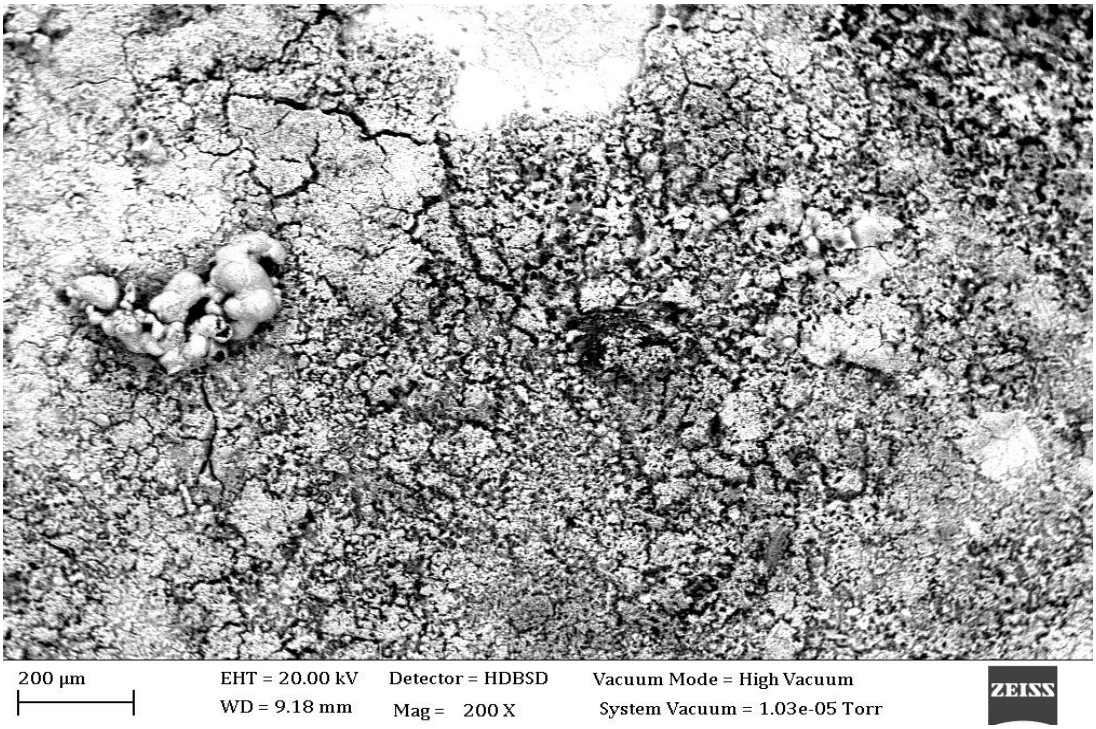

Figure 15: SEM image of Zn-MgO30-Al_2O_3 (15 mins)

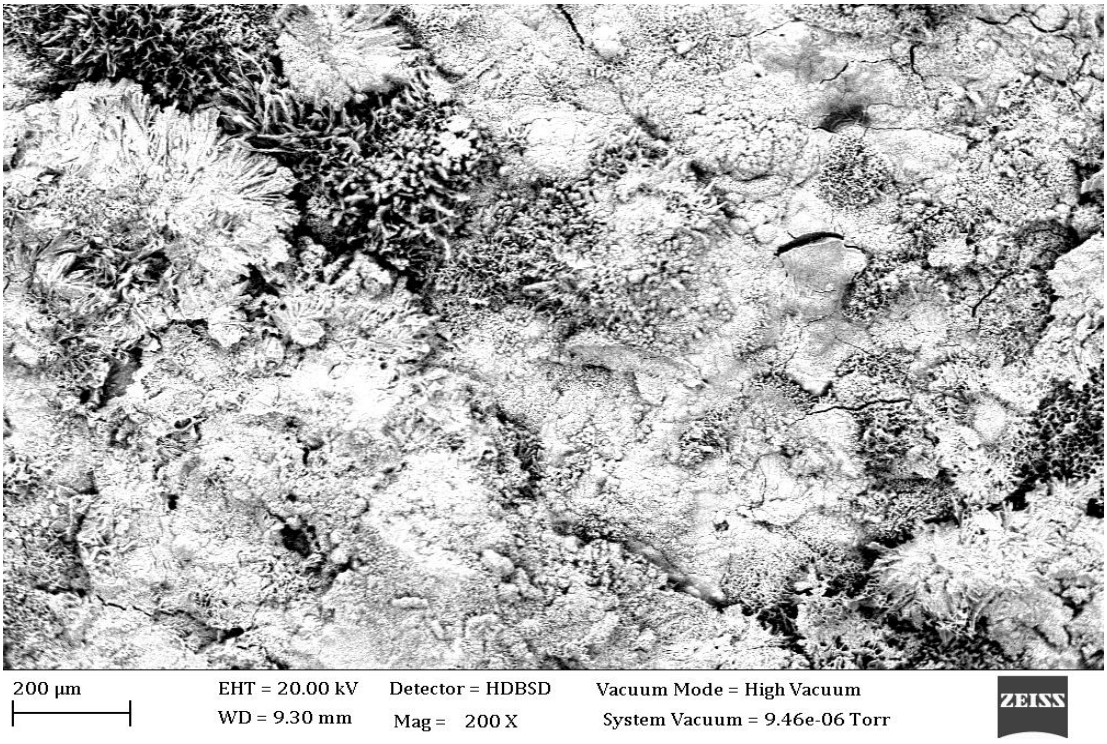

Figure 16: SEM image of Zn-MgO30-Al_2O_3 (20 mins)

4. Conclusions

This research was carried out to investigate the effect of deposition time variation and mass concentration of MgO on the corrosion response and microstructure of Zn-MgO-Al_2O_3 coated mild steel. The following conclusions are drawn from the study:

(i) The variation in the deposition time and mass concentration of MgO had a significant effect on corrosion resistance and microstructure of the coatings. The increment in the mass concentration of MgO and deposition time up to optimum values enhanced the corrosion resistance and microstructural properties of the Zn-MgO-Al_2O_3 coatings.

(ii) The uncoated sample exhibited the least corrosion resistance, with the corrosion rate and corrosion current density of 20.707 mm/year and 1782 μA/cm^2, respectively. The steel coated with Zn-MgO30-Al_2O_3 (20 mins) exhibited the optimum corrosion resistance, with the corrosion rate and corrosion current density of 1.0521 mm/year and 90.51 μA/cm^2, respectively. This showed that the coating reduced the attack of the steel surface by the 3.5% wt. NaCl solution.

(iii) The coatings were observed to exhibit refined morphology with compact, granulated, flower-flake-like and flower-nodule-like structures, which were found beneficial to the corrosion properties of the coating.

Acknowledgement

The SEM used in this study was provided by Matrix Energy Laboratory (MEL), Department of Materials Science and Engineering, Obafemi Awolowo University, Ile-Ife, Nigeria. The authors of this paper gratefully acknowledge the immense support received from the management of MEL in this work.

References

[1] Neukirchen, F., Ries, G., Neukirchen, F., & Ries, G. (2020). The World of Metals. The World of Mineral Deposits: A Beginner's Guide to Economic Geology, 51-80.

[2] Ramlee, E. B., Hussain, P. B., & Shaik, N. B. (2020). Enhancing the lifetime and corrosion resistance of gears made of carbon steel. Materialwissenschaft und Werkstofftechnik, 51(6), 774-779.

[3] Fayomi, O. S. I., Akande, I. G., & Ofo, C. (2021). Investigation of corrosion resistance and microstructural performance of Zn-MgO-WB composite coating on mild steel. In Key Engineering Materials (Vol. 886, pp. 159-167). Trans Tech Publications Ltd.

[4] Yu, Y., Lan, L., Ding, F., & Wang, L. (2019). Mechanical properties of hot-rolled and cold-formed steels after exposure to elevated temperature: A review. Construction and Building Materials, 213, 360-376.

[5] Khurshid, M., Leitner, M., Barsoum, Z., & Schneider, C. (2017). Residual stress state induced by high frequency mechanical impact treatment in different steel grades–Numerical and experimental study. International Journal of Mechanical Sciences, 123, 34-42.

[6] Oyyaravelu, R., Kuppan, P., & Arivazhagan, N. (2016). Metallurgical and mechanical properties of laser welded high strength low alloy steel. Journal of advanced research, 7(3), 463-472.

[7] Singh, G. (2021). A review on effect of heat treatment on the properties of mild steel. Materials Today: Proceedings, 37, 2266-2268.

[8] Mathew, M., & Rajendrakumar, P. K. (2011). Optimization of process parameters of boro-carburized low carbon steel for tensile strength by Taquchi method with grey relational analysis. Materials & Design, 32(6), 3637-3644.

[9] Toutov, A. A., Liu, W. B., Betz, K. N., Fedorov, A., Stoltz, B. M., & Grubbs, R. H. (2015). Silylation of C–H bonds in aromatic heterocycles by an Earth-abundant metal catalyst. Nature, 518(7537), 80-84.

[10] Verma, C., Ebenso, E. E., Bahadur, I., & Quraishi, M. A. (2018). An overview on plant extracts as environmental sustainable and green corrosion inhibitors for metals and alloys in aggressive corrosive media. Journal of molecular liquids, 266, 577-590.

[11] Akande, I. G., Oluwole, O. O., & Fayomi, O. S. I. (2019). Optimizing the defensive characteristics of mild steel via the electrodeposition of $ZnSi_3N_4$ reinforcing particles. Defence Technology, 15(4), 526-532.

[12] Güral, A., Bostan, B., & Özdemir, A. T. (2007). Heat treatment in two phase region and its effect on microstructure and mechanical strength after welding of a low carbon steel. Materials & design, 28(3), 897-903.

[13] Cao, T. S., Bobadilla, C., Montmitonnet, P., & Bouchard, P. O. (2015). A comparative study of three ductile damage approaches for fracture prediction in cold forming processes. Journal of Materials Processing Technology, 216, 385-404.

[14] Takahashi, S., Kobayashi, S., Tomáš, I., Dupre, L., & Vértesy, G. (2017). Comparison of magnetic nondestructive methods applied for inspection of steel degradation. NDT & E International, 91, 54-60.

[15] Ajide, O. O., Onakoya, O., Akande, I. G., Saxena, K. K., Mohammed, K. A., & Kumar, N. (2022). Fatigue Life Examination and Crack Propagation characteristics of two Ferrous based Alloy materials. International Journal on Interactive Design and Manufacturing (IJIDeM), 1-7.

[16] Yu, C., Dong, B., Chen, Y. F., Ma, B. Y., Ding, J., Deng, C. J., ... & Di, J. H. (2022). Enhanced oxidation resistance of low-carbon MgO–C refractories with ternary carbides: a review. Journal of Iron and Steel Research International, 29(7), 1052-1062.

[17] Chen, B., Shen, J. H., Ye, X. X., Jia, L., Li, S. F., Umeda, J., ... & Kondoh, K. (2017). Length effect of carbon nanotubes on the strengthening mechanisms in metal matrix composites. Acta Materialia, 140, 317-325.

[18] Liu, Q., Liu, X., Feng, H., Shui, H., & Yu, R. (2017). Metal organic framework-derived Fe/carbon porous composite with low Fe content for lightweight and highly efficient electromagnetic wave absorber. Chemical Engineering Journal, 314, 320-327.

[19] Narasimharaju, S. R., Zeng, W., See, T. L., Zhu, Z., Scott, P., Jiang, X., & Lou, S. (2022). A comprehensive review on laser powder bed fusion of steels: Processing, microstructure, defects and control methods, mechanical properties, current challenges and future trends. Journal of Manufacturing Processes, 75, 375-414.

[20] Ikeuba, A. I., Agobi, A. U., Hitler, L., Omang, B. J., Asogwa, F. C., Benjamin, I., ... & Udoinyang, M. C. (2023). Green approach towards corrosion inhibition of mild steel during acid pickling using chlorpheniramine: experimental and DFT study. Chemistry Africa, 6(2), 983-997.

[21] Raabe, D. (2023). The materials science behind sustainable metals and alloys. Chemical Reviews, 123(5), 2436-2608.

[22] Xavier, J. R. (2023). Improvement in corrosion resistance and mechanical properties of epoxy coatings on steel with the addition of thiadiazole treated ZrC. Journal of Materials Engineering and Performance, 32(9), 3980-3994.

[23] Al Shibli, F. S. Z. S., Bose, S., Kumar, P. S., Rajasimman, M., Rajamohan, N., & Vo, D. V. N. (2021). Green technology for sustainable surface protection of steel from corrosion: a review. Environmental Chemistry Letters, 1-19.

[24] Rosliza, R. (2012). Improvement of corrosion resistance of aluminium alloy by natural products (Vol. 55, pp. 62-69). InTech.

[25] Akande, I. G., Fayomi, O. S. I., & Akpan, B. J. (2022). Development of UPP nanoparticles reinforced Zn–ZnO–MgO composite coating for corrosion-resistance, hardness, and microstructure property enhancement of AISI 1015 carbon steel for

automotive and marine applications. The International Journal of Advanced Manufacturing Technology, 123(3-4), 999-1008.

[26] Rosso, M., Peter, I., & Gobber, F. S. (2015). Overview of heat treatment and surface engineering, influences of surface finishing on hot–work tool steel. International Journal of Microstructure and Materials Properties, 10(1), 3-30.

[27] Sadananda, K., Yang, J. H., Iyyer, N., Phan, N., & Rahman, A. (2021). Sacrificial Zn–Ni coatings by electroplating and hydrogen embrittlement of high-strength steels. Corrosion Reviews, 39(6), 487-517.

[28] Choudhary, R. K., Mishra, P., & Kain, V. (2017). Pulse DC electrodeposition of Zn–Ni–Co coatings. Surface Engineering, 33(2), 90-93.

[29] Adhilakshmi, A., Ravichandran, K., & TSN, S. N. (2020). Cathodic electrodeposition of zinc–zinc phosphate–calcium phosphate composite coatings on pure iron for biodegradable implant applications. New Journal of Chemistry, 44(16), 6475-6489.

[30] Hayatdavoudi, H., & Rahsepar, M. (2017). A mechanistic study of the enhanced cathodic protection performance of graphene-reinforced zinc rich nanocomposite coating for corrosion protection of carbon steel substrate. Journal of Alloys and Compounds, 727, 1148-1156.

[31] Yasoda, R. D., Huang, Y., & Qi, X. (2022). Corrosion Performance of Wire Arc Deposited Zinc Aluminum Pseudo Alloy and Zinc 15 Aluminum Alloy Coatings on Steel in Chloride Environment. Journal of Thermal Spray Technology, 31(6), 1918-1933.

[32] Nazarov, A., Le Bozec, N., & Thierry, D. (2018). Scanning Kelvin Probe assessment of steel corrosion protection by marine paints containing Zn-rich primer. Progress in Organic Coatings, 125, 61-72.

[33] Klenam, D. E., Bodunrin, M. O., Akromah, S., Gikunoo, E., Andrews, A., & McBagonluri, F. (2021). Ferrous materials degradation: characterisation of rust by colour–an overview. Corrosion Reviews, 39(4), 297-311.

[34] Melchers, R. E. (2021). Long-term corrosion of steels in deep, cold, low oxygen sea waters. Corrosion Engineering, Science and Technology, 56(8), 736-741.

[35] Yuan, W., Xia, D., Wu, S., Zheng, Y., Guan, Z., & Rau, J. V. (2022). A review on current research status of the surface modification of Zn-based biodegradable metals. Bioactive materials, 7, 192-216.

[36] Kwon, M., Jo, D. H., Cho, S. H., Kim, H. T., Park, J. T., & Park, J. M. (2016). Characterization of the influence of Ni content on the corrosion resistance of electrodeposited Zn–Ni alloy coatings. Surface and Coatings Technology, 288, 163-170.

[37] Keyvani, A., Yeganeh, M., & Rezaeyan, H. (2017). Electrodeposition of Zn-Co-Mo alloy on the steel substrate from citrate bath and its corrosion behavior in the chloride media. Journal of Materials Engineering and Performance, 26, 1958-1966.

[38] Yang, G., Wang, B., Tawfiq, K., Wei, H., Zhou, S., & Chen, G. (2017). Electropolishing of surfaces: theory and applications. Surface Engineering, 33(2), 149-166.

[39] Hassani-Gangaraj, S. M., Moridi, A. T. I. E. H., & Guagliano, M. A. R. I. O. (2015). Critical review of corrosion protection by cold spray coatings. Surface Engineering, 31(11), 803-815.

[40] Eduok, U., Faye, O., & Szpunar, J. (2017). Recent developments and applications of protective silicone coatings: A review of PDMS functional materials. Progress in Organic Coatings, 111, 124-163.

[41] Jiang, C. C., Cao, Y. K., Xiao, G. Y., Zhu, R. F., & Lu, Y. P. (2017). A review on the application of inorganic nanoparticles in chemical surface coatings on metallic substrates. RSC advances, 7(13), 7531-7539.

[42] BILGIC, S. (2018). The methods for prevention of corrosion. The Eurasia Proceedings of Science Technology Engineering and Mathematics, (4), 182-186.

[43] Qu, J., Meyer III, H. M., Cai, Z. B., Ma, C., & Luo, H. (2015). Characterization of ZDDP and ionic liquid tribofilms on non-metallic coatings providing insights of tribofilm formation mechanisms. Wear, 332, 1273-1285.

[44] Shibli, S. M. A., Meena, B. N., & Remya, R. (2015). A review on recent approaches in the field of hot dip zinc galvanizing process. Surface and Coatings Technology, 262, 210-215.

[45] Pokorny, P., Kolisko, J., Balik, L., & Novak, P. (2016). Reaction kinetics of the formation of intermetallic Fe–Zn during hot-dip galvanizing of steel. Metalurgija, 55(1), 111-114.

[46] Rizvi, M. A. (2015). Complexation modulated redox behavior of transition metal systems. Russian Journal of General Chemistry, 85, 959-973.

[47] Cetinkaya, B. W., Junge, F., Mueller, G., Haakmann, F., Schierbaum, K., & Giza, M. (2020). Impact of alkaline and acid treatment on the surface chemistry of a hot-dip galvanized Zn–Al–Mg coating. Journal of Materials Research and Technology, 9(6), 16445-16458.

[48] Costa, A. N. C., Silva, G. C., Ferreira, E. A., & Nakazato, R. Z. (2021). Comparative analysis of corrosion resistance of Zinc and Zn-Al-Mg coatings on carbon steel. Research, Society and Development, 10(1), e49810111973-e49810111973.

[49] Hasnidawani, J. N., Azlina, H. N., Norita, H., Bonnia, N. N., Ratim, S., & Ali, E. S. (2016). Synthesis of ZnO nanostructures using sol-gel method. Procedia Chemistry, 19, 211-216.

[50] Weckman, T., & Laasonen, K. (2016). Atomic layer deposition of zinc oxide: diethyl zinc reactions and surface saturation from first-principles. The Journal of Physical Chemistry C, 120(38), 21460-21471.

[51] Nikoofar, K., Shahedi, Y., & Chenarboo, F. J. (2019). Nano alumina catalytic applications in organic transformations. Mini-Reviews in Organic Chemistry, 16(2), 102-110.

[52] Gangwar, J., Gupta, B. K., Tripathi, S. K., & Srivastava, A. K. (2015). Phase dependent thermal and spectroscopic responses of Al_2O_3 nanostructures with different morphogenesis. Nanoscale, 7(32), 13313-13344.

[53] Akande, I. G., Fayomi, O. S. I., Akpan, B. J., Aogo, O. A., & Onwordi, P. N. (2022). Exploration of the effect of Zn-MgO-UPP coating on hardness, corrosion resistance and microstructure properties of mild steel. Journal of Electrochemical Science and Engineering, 12(5), 829-840.

[54] Xu, Z., Eduok, U., & Szpunar, J. (2019). Effect of annealing temperature on the corrosion resistance of MgO coatings on Mg alloy. Surface and Coatings Technology, 357, 691-697.

[55] Thiruvoth, D. D., & Ananthkumar, M. (2022). Evaluation of cerium oxide nanoparticle coating as corrosion inhibitor for mild steel. Materials Today: Proceedings, 49, 2007-2012.

[56] Patra, R., Gautam, A., Gobi, K. V., & Subasri, R. (2023). Hybrid Silane Coatings Based on Benzotriazole Loaded Aluminosilicate Nanotubes for Corrosion Protection of Mild Steel. Silicon, 1-16.

[57] Xu, P., Zhao, M., Fu, X., & Zhao, C. (2022). Effect of chloride ions on the corrosion behavior of carbon steel in an iron bacteria system. RSC advances, 12(24), 15158-15166.

[58] Li, B., Li, D., Chen, W., Liu, Y., Zhang, J., Wei, Y., ... & Jia, W. (2019). Effect of current density and deposition time on microstructure and corrosion resistance of Ni-W/TiN nanocomposite coating. Ceramics International, 45(4), 4870-4879.

[59] Dai, C. D., Fu, Y., Guo, J. X., & Du, C. W. (2020). Effects of substrate temperature and deposition time on the morphology and corrosion resistance of $FeCoCrNiMo_{0.3}$ high-entropy alloy coating fabricated by magnetron sputtering. International Journal of Minerals, Metallurgy and Materials, 27, 1388-1397.

[60] Zhou, J., & Kong, D. (2019). Effects of Ni addition on corrosion behaviors of laser cladded FeSiBNi coating in 3.5% NaCl solution. Journal of Alloys and Compounds, 795, 416-425.

[61] Fayomi, O. S. I., Akande, I. G., Popoola, A. P. I., Popoola, S. I., & Daramola, D. (2019). Structural characterization and corrosion properties of electroless processed $NiPMnO_2$ composite coatings on SAE 1015 steel for advanced applications. Journal of Science: Advanced Materials and Devices, 4(2), 285-289.

[62] Chen, X., Wang, H., Wang, C., Zhang, W., Lv, C., & Zhu, Y. (2019). A novel antiscaling and anti-corrosive polymer-based functional coating. Journal of the Taiwan Institute of Chemical Engineers, 97, 397-405.

[63] Ding, J. H., Zhao, H. R., Zheng, Y., Zhao, X., & Yu, H. B. (2018). A long-term anticorrsive coating through graphene passivation. Carbon, 138, 197-206.

[64] Zhang, Y., Shao, Y., Liu, X., Shi, C., Wang, Y., Meng, G., ... & Yang, Y. (2017). A study on corrosion protection of different polyaniline coatings for mild steel. Progress in Organic Coatings, 111, 240-247.

[65] Athira, R., Poongothai, N., Neena, P. K., Babu, T. S., & Stanley, J. (2018). Study of corrosion protection effect of low cost bio extract-polymer coating material for mild steel in acidic and marine environments-a cost effective approach. Int J Eng Technol, 7, 315-21.

[66] Hamidon, T. S., Ishak, N. A., & Hussin, M. H. (2021). Enhanced corrosion inhibition of low carbon steel in aqueous sodium chloride employing sol–gel-based hybrid silanol coatings. Journal of Sol-Gel Science and Technology, 97, 556-571.

[67] Hsissou, R., Benhiba, F., Dagdag, O., El Bouchti, M., Nouneh, K., Assouag, M., ... & Elharfi, A. (2020). Development and potential performance of prepolymer in corrosion inhibition for carbon steel in 1.0 M HCl: Outlooks from experimental and computational investigations. Journal of colloid and interface science, 574, 43-60.

[68] Wang, Y., & Zuo, Y. (2017). The adsorption and inhibition behavior of two organic inhibitors for carbon steel in simulated concrete pore solution. Corrosion Science, 118, 24-30.

[69] Yeganeh, M., Asadi, N., Omidi, M., & Mahdavian, M. (2019). An investigation on the corrosion behavior of the epoxy coating embedded with mesoporous silica nanocontainer loaded by sulfamethazine inhibitor. Progress in Organic Coatings, 128, 75-81.

[70] Veisi, H., Mohammadi, L., Hemmati, S., Tamoradi, T., & Mohammadi, P. (2019). In situ immobilized silver nanoparticles on rubia tinctorum extract-coated ultrasmall iron oxide

nanoparticles: an efficient nanocatalyst with magnetic recyclability for synthesis of propargylamines by A3 coupling reaction. ACS omega, 4(9), 13991-14003.

[71] Pour, Z. S., Ghaemy, M., Bordbar, S., & Karimi-Maleh, H. (2018). Effects of surface treatment of TiO2 nanoparticles on the adhesion and anticorrosion properties of the epoxy coating on mild steel using electrochemical technique. Progress in Organic Coatings, 119, 99-108.

[72] Xavier, J. R. (2021). Electrochemical and mechanical investigation of newly synthesized NiO-ZrO_2 nanoparticle–grafted polyurethane nanocomposite coating on mild steel in chloride media. Journal of Materials Engineering and Performance, 30(2), 1554-1566.

[73] Peng, T., Xiao, R., Rong, Z., Liu, H., Hu, Q., Wang, S., ... & Zhang, J. (2020). Polymer Nanocomposite-based Coatings for Corrosion Protection. Chemistry–An Asian Journal, 15(23), 3915-3941.